Carbonaceous Nanoparticle Layers Prepared using Candle Soot by Direct- and Spray-based Depositions

Ferry Faizal[1], M.P. Khairunnisa[1,2], Shunichiro Yokote[2], I. Wuled Lenggoro[1,3*]

[1] *Graduate School of Bio-Applications and Systems Engineering, Tokyo University of Agriculture and Technology, Koganei, Tokyo 184-8588, Japan*
[2] *Malaysia - Japan International Institute of Technology, Universiti Teknologi Malaysia, 54100 Kuala Lumpur, Malaysia*
[3] *Department of Chemical Engineering, Tokyo University of Agriculture and Technology, Koganei, Tokyo 184-8588, Japan*

ABSTRACT

To investigate the properties and structures of soot particles derived from candle combustion, two deposition routes were performed. In "Route-1," the aerosol (soot) particles were collected by direct exposure of a substrate in a chamber with controlled airflows. In "Route-2," deposited soot nanoparticles was transferred into suspension and subsequently, the deposition of particles on to the substrate was achieved by an electrospray. Raman spectral analysis has shown the difference of G-band intensity relative to D-band between hydrophobic and hydrophilic particle layers obtained from different collection regions of the candle flame. It also reveals the effect of airflows during the collection to the ratio of the D to G peak. Meanwhile, the Raman spectra of the particles seem invariant to the preparation methods of suspension and electrospray deposition process. From the curve gradient of spectroscopy (190–2500 nm) results, the electrospray-deposited particle layers (Route-2) show higher absorbance in the near-infrared region compared to direct-deposited particle layers (Route-1). This change in the spectrum may due to the change in morphology of nanoparticle layers formed by each route.

Keywords: Aerosol deposition; Carbonaceous aerosols; Nanostructured materials; Optical spectroscopy; Soot.

INTRODUCTION

The investigation of soot characteristic derived from combustion systems has drawn increasing attention. In relation to the basic properties characterization and structural investigation, many studies have been performed by considering various factors such as sources, the formation process, structures, and further treatments (Ferrari and Robertson, 2000; Popovicheva *et al.*, 2014; Nithyanandan *et al.*, 2016). In the structural studies, graphite-like and the diamond-like hybrid orbital composition, mainly drive the properties of carbon allotropes (Osswald *et al.*, 2006). The same theoretical aspects are also applied to the soot and "carbon black" particles, which are generally produced by thermal decomposition of hydrocarbon fuel (Long *et al.*, 2013). The content and proportion of the hybrid orbital bonds determine the mechanical properties such as hardness, electrical conductivity, and heat conductivity (Falcao and Wudl, 2007).

Recently, considering the unique structure of carbonaceous materials such as graphene, carbon nanotube, and fullerene, soot particles derived from hydrocarbon combustion have also caught attention in the development of the composite materials with unique properties. For instance, carbonaceous (soot) nanoparticles derived from burning candle have been applied as the anode of Li-ion batteries with high surface area and porosity (Kakunuri and Sharma, 2015). This effort can be seen as seeking a simple alternative material for the conducting agent in battery systems. On the other hand, hydrophobic properties of candle-soot-derived particle layers have also been investigated, and they exhibit a super-hydrophobic effect, which may correlate to the organic content, aggregate size, and the bond structure (Liang *et al.*, 2014; Sahoo and Kandasubramanian, 2014).

Bescond *et al.* (2016) investigated the optical properties of soot particle derived from ethylene diffusion flame by analyzing the specific extinction coefficient at the near-UV region, while the effect of the water coating to the optical properties was also reported (Fan *et al.*, 2016). Another report correlated optical properties of soot particles with the molecular weight of the species in premix flame-type combustion of ethylene/O_2 and benzene/N_2/O_2 (Russo *et*

---
*Corresponding author.
Tel.: +81-42-388-7987
E-mail address: wuled@cc.tuat.ac.jp

al., 2013). The characterization of indoor particle emission from candle burning was comprehensively discussed in another study (Fine *et al.*, 1999).

As an application of candle soot particles as a functional material, it was reported that bilayers composite of candle soot-polydimethylsiloxane (PDMS) can efficiently convert the high photonic energy of laser into an acoustic wave at ultrasonic frequency (Chang *et al.*, 2015). Those results show the excellent optical absorption properties of candle soot particles and their capability to convert the photonic energy into local heating phenomena. It then can be considered that it is critical to investigate optical characteristics of soot nanoparticle (layers) derived from combustion (e.g., candle burning) because the structural bond is fairly sensitive to the formation process during combustion.

In the present study, we investigated two routes for collecting and deposition of candle soot particles. Route-1 is a well-reported method of depositing particles on to a substrate collector substrate directly from a candle flame. This method is useful since the layered particles are "original." However, it is not easy to control the growth process of the layer on the substrate. Route-2 is based on the dispersion of the collected particles on the substrate (in Route-1) into a polar medium (water or ethanol) to become a suspension. The suspension is then spray-deposited on to a substrate. One of the objectives is to clarify whether the suspension preparation, aerosolization, and deposition processes affect the properties of carbonaceous nanoparticle layers. The present work is also intended to contribute to a better controllable deposition method and particle-layer growth for further applications (e.g., functional materials) and to build a deeper understanding of the soot particles derived from combustion processes.

METHODS

Direct Deposition (Route-1)

An experimental system has been developed to directly deposit the soot particles from candle flame, which is classified as a non-premixed burner (in others references, the term of diffusion flame are used) (Bescond *et al.*, 2016; Oh and Shin, 2006; Wu *et al.*, 2017). The set up simply utilizes semi-open glass tube (inner diameter = 47 mm, length = 199 mm) equipped with candle position control by utilizing smooth mechanical shifting by a syringe pump. The system was intended to maintain a constant position of collecting substrate relative to the position of the wick. The position of the substrate was following some previous work by others (Sahoo and Kandasubramanian, 2014; Kakunuri and Sharma, 2015). This could be critical since the properties of the soot deposited from the interior of the flame exhibit super-hydrophobic properties and the soot from tips of the flame show a hydrophilic nature. The argumentation for the cause of the phenomena in those studies focuses on the average size and organic content of the soot particle. Meanwhile, another factor, the role of different O_2 content in flame position, remains unclear. In the present study, the effort to control O_2 content was performed by controlling airflow rate. Dry air was delivered at various rates (3–

13 L min⁻¹) from the bottom of the tube as a supply of the O_2 reactant in the candle flame. The deposition time is five minutes for each flow rate. On the other hand, the size distributions of particles suspended in the gas-phase (as aerosols) were measured by an online sizing system (SMPS, TSI Inc., USA). The measured sizes of the generated aerosols were between a few tens and few hundreds of nanometers (not shown). These results were obtained when the candle was surrounded by a glass tube (diameter 44 mm). By placing a probe (conductive resin, diameter 6 mm) at some positions around or above the flame, the suction speed was 0.6 m s⁻¹.

On the top of the tube, a fine mesh grid (0.25 mm²) of metal was mounted to prevent ambient air flow from the outside in such a way that if the air flows were cut off, the flame would be shut down. In the experiment using the tube dimension mentioned above, the cut-off flow rate or flame dead zone is at flow rates less than 3 L min⁻¹ of air regulator. The collection scheme is illustrated in Fig. 1. Paraffin wax candles (diameter = 9 mm, length 100 mm) were used as the sources. Glass plates (Pyrex, 25 × 25 × 1.3 mm, Sansyo Co. Ltd., Japan) were used as collecting substrates. To determine deposition rate, the mass balance between that of initial glass plates and that after the particles deposited in the same interval of time (5 min) were measured.

Deposited particle layers were analyzed by Raman spectroscopy (Micro-Raman Almega, Thermofischer Scientific, USA). The hydrophobicity was measured by contact angle meter (DM-501, KYOWA, Japan) and optical properties of the layers were analyzed by UV-Vis-NIR spectrometer (MSV-370, JASCO, Japan).

Preparation of Soot Suspension

Deposited soot particles (flame interior soot particle) were dispersed in ethanol (99.5%, Wako Chemical, Japan) with ultrasonic homogenization (23 KHz for 10 min and 43 kHz for 10 min) until well-dispersed "ink like" suspension was formed. The particle size distributions of the deposited particles as suspension of ethanol and ultrapure water were analyzed using a Dynamic Light Scattering instrument (DLS, Zetasizer Nano-ZS, Malvern, UK) at different concentrations.

Electrospray Deposition (Route-2)

Electrospray method was chosen as the aerosolization method for suspension because it covers a distribution of a wide range of particle sizes and has been proven to have relatively sensitive content in aerosol droplet—for example, biomolecule and enzyme (Fenn *et al.*, 1989; Saallah *et al.*, 2014). It is also considered a reasonable deposition method that can minimize the change of properties of soot particles contained in aerosol droplets before their deposition on the substrate. Experimental condition for the electrospray deposition is as follows. The soot suspension in ethanol was sprayed by electrospray method in cone-jet mode (Lenggoro *et al.*, 2002) from the nozzle (a metal capillary tube, ID:0.42, OD:0.65 mm) to the grounded aluminum foil. Stable cone-jet mode was achieved in a 2.4–2.6 kV
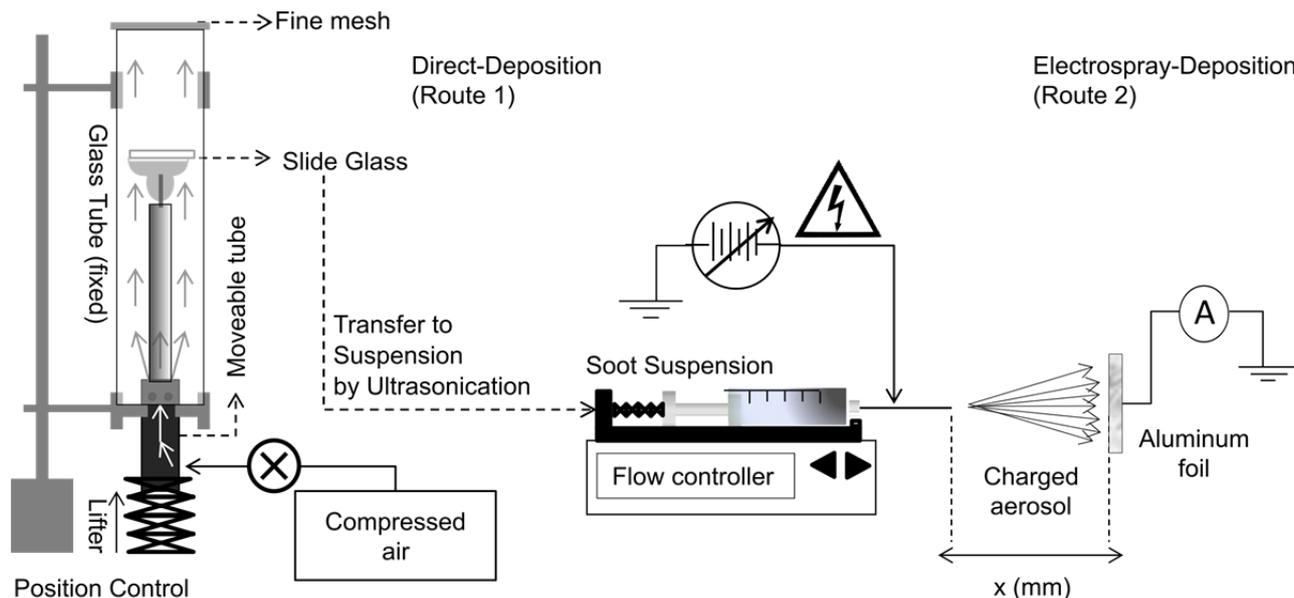
Fig. 1. Experimental scheme: Route-1 (Direct) and Route-2 (Electrospray of soot suspension).

range (for a nozzle-to-substrate distance of 23 cm and flowrate 0.1 mL h^{-1}). Deposition time was varied to 5, 10, 15, and 20 min as the representation of layer-thickness variation. The deposition was conducted in 18–19°C (room temperature) at 57–59% relative humidity and standard atmospheric pressure. The suspension concentration was 0.18 wt % (soot) particles in ethanol. Ethanol was chosen instead of water to ensure an "easier" spraying condition, the higher evaporation rate of the droplet allowing faster drying than water solvent at room temperature.

RESULTS AND DISCUSSION

Hydrophobicity and Morphology

Hydrophobic properties of deposited soot have shown distinct characteristic related to the position of collection (slide glass in Fig. 1). Flame tip position was also used as a comparison to the main (center) flame interior position for collecting the soot particles.

The contact angle (CA) measurement shows that the average value of water droplet CA on the layer of deposited soot particle has the average value of 151 + 1.3 degrees for soot deposited from the flame interior. For tip position, the average value of 5.23 + 0.9 degrees exhibits properties of the hydrophilic layer. The screenshots of the droplet shape on the surface of the layers are presented in Fig. 2. The comparison shows distinct properties in agreement with other study of candle soot (Sahoo and Kandasubramanian, 2014). Static CA measurements of particle layers are summarized in Table 1. Zero mins for Route-2 means the values belong to the substrate (Al) showing hydrophilic properties. After 5-min spray, the CA increased up to 121° then decreased with operation-time. The results may correlate to increasing thickness and change in surface roughness. Compared to the layer obtained by Route-1 (with the position of the flame interior), the Route-2 layer cannot reach the values of the original order < 150°. This might be due

to the change in morphology as the effect of the deposition time (Fig. 3, Route 2).

Super-hydrophobic phenomena are mainly related to the existence of more organic compounds or functional surface present in the particulate layer obtained from interior flame and the size effect of the soot particle (Liang *et al.*, 2014). The properties of flame in the different regions of candle soot flame are rarely discussed. For the premixed type ethylene-air burner, an experimental study of the hydrophobic properties has shown the different static contact angle from richer flame region with leaner flame region (Commodo *et al.*, 2016). One reference discusses that the insufficient oxygen region appears in the yellow bright part of the flame. That the oxygen deficiency is the main cause of generation of larger soot particle has been shown experimentally by Pagels (Pagels *et al.*, 2009) and an older study in diesel soot by Haynes and Wagner (Haynes and Wagner, 1981).

The morphologies of the soot particles are presented in Fig. 3. For Route-1, the morphologies and primary particle size of the soot obtained from the tip are almost identical with those of the interior of flame. Primary particles (less than 100 nm) were observed in the form of their aggregates, which is a well-known structure (Skorupski and Mroczka, 2014).

The results of Route-2 have shown heavily aggregated by necking and overlapping structure. Overall, the size of primary particles is larger those of Route-1. Because the liquid route is used, larger (primary) particles may indicate the "active" properties of soot due to the adsorption of matters in the liquid samples, and the phenomena are discussed elsewhere (Weingartner *et al.*, 1997). The contribution of the necking and overlapping of primary particles will be discussed in the optical properties section.

Raman Spectroscopy

The present results suggest that the structural bond of soot particles contributes to the hydrophobic properties of particle layers. This hypothesis can be indicated by the

(a)   (b)
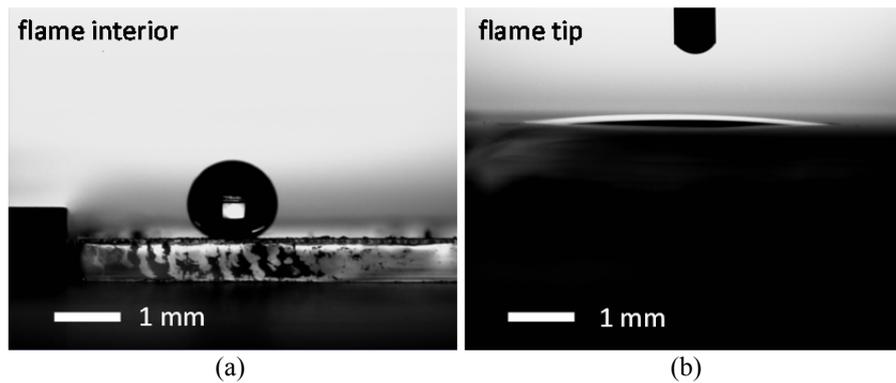
Fig. 2. Droplet drop screenshot: round water droplet shape preserved in the case of particle layer derived from the flame interior (a) and droplet absorbed by the layer of particles derived from the flame tip (b).

Table 1. Contact angle (CA) measurement of particle layers.

Time (min)	Static CA (°)	Deposition type/notes
0	73.3 ± 1.6	Route 2/substrate only
5	121.8 ± 1.7	Route 2
10	120.0 ± 1.6	Route 2
15	107.2 ± 1.0	Route 2
20	104.3 ± 1.4	Route 2
5	151.0 ± 1.3	Route 1, from flame interior
5	5.2 ± 0.9	Route 1, from flame tips
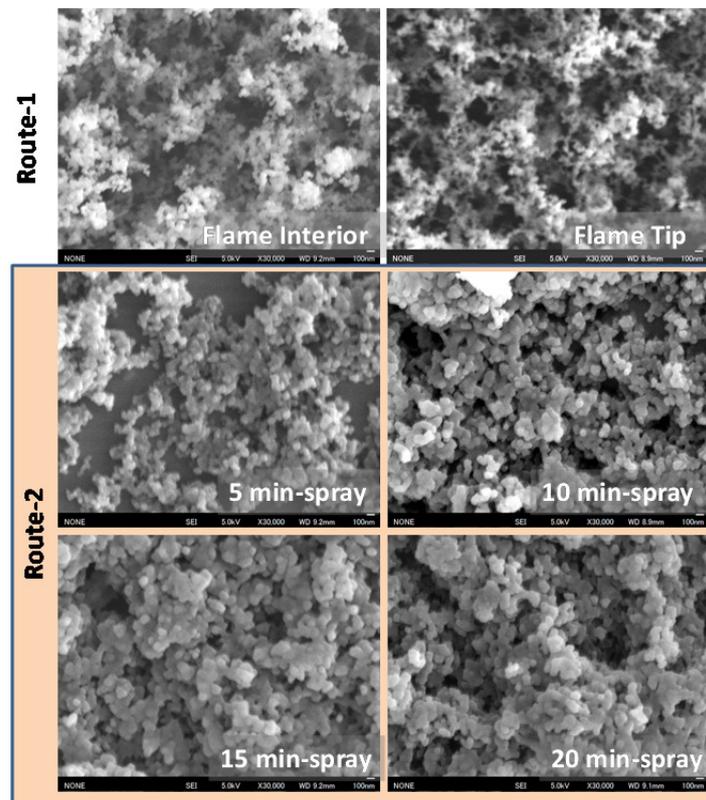
Fig. 3 Morphologies of deposited particle layers, prepared by Route-1 and Route-2, at different deposition (spraying) times.

intensity of the G-peak in Raman spectra (Fig. 4(a)). There are different peak ratios between particle layers deposited from the flame interior and flame tips. In the case of layers from the flame interior, Raman (peak) intensity of D-band and G-band are unequal. Raw G-band peaks are higher compared to the D-band peaks. One can roughly describe

that there is a more-graphitic-like structure in the soot particle layers derived from the flame interior. This result indicates the well-known hydrophobic properties of graphite (Yang and Zewail, 2009).

As presented in Fig. 4(a), the Raman spectrum differs significantly between the layers derived from the interior and tip of the flames (in Route 1). Meanwhile, the next-step processes (suspension preparation and electrospray deposition) for Route-2 are invariant to the shape of the Raman spectrum (Fig. 4(b)), which is indicated by the preservation of the intensity ratio of G and D-bands. There is a change in relative intensity due to short deposition time (Fig. 4(b), 0.5 min). Deposition in shorter time indicates the stronger intensity of Raman spectra, compared with those of longer time deposition. This may be because the lower-density particles (the morphologies of the layer as presented in Fig. 3, route 2) enhanced the (Raman) scattering process by interference (Ramsteiner *et al.*, 1989). In the case of the rough bulk layer, the scattering energy was absorbed more by particles (Sovány *et al.*, 2009).

To investigate the effects of flow in the soot particle formations, we performed decomposition of the Raman spectrum in the 600–2000 cm^{-1} region and fitting the cumulative superposition curve to the observed Raman spectrum following the method described in several references (Ferrari and Robertson, 2000; Sadezky *et al.*, 2005; Cançado *et al.*, 2006). The decomposition steps consist of choosing the peak candidate of peak components. The peak function usually consists of a Gaussian function or Lorentzian function located in the different locations in wavenumber domain. The curve-fitting was iterated by comparing component superposition (cumulative curve) with the measured curve until the smallest residual between both curves was achieved.

Following the work of Sadezky *et al.* (2005) initial peaks location and function was divided into the specific bands (D1, 1360 cm^{-1}; D2, 1620 cm^{-1}; D3, 1500 cm^{-1}; D4, 1180 cm^{-1}; and G, 1580 cm^{-1}) with all Lorentzian (Cauchy function) except for D3 (Gaussian function shape).

In the fitting process, we set all parameters (peak center, bandwidth, intensity, and background) free for optimum fitting. One example of calculation result of open chamber (no flow rate control) flame soot collection is presented in Table 2 and the curves plot is presented in Fig. 5. In the decomposition calculation steps, the D2 band was shifting significantly to 2000 cm^{-1}. However, it is also possible to consider the band as belongs to the C-C band (Casari *et al.*, 2008) as the presence of sp-hybridized carbon atom of a C-C stretching bond, indicated by several wiggles at the 1800–2100 cm^{-1} region.

The decomposition procedures were repeated for other flow rate values. The plots of D1/G ratio versus airflow rate during particle collection/deposition are presented in Fig. 6(b). In the case of the open chamber, the D1/G ratio is close to 1. At 3–9 L min^{-1}, the ratios were increasing then subsequently dropped at 11 L min^{-1}. To explain the phenomena, we compared the plots of Fig. 6(b) with Fig. 6(a). Fig. 6(a) shows the deposition rate obtained by mass balance measurement of the collecting substrate versus airflow rate. The region less than 3 L min^{-1} is the "dead zone" of the flame. The flows between 3–9 L min^{-1} are steady flame, and those above 11 L min–1 make the flame flicker, indicating a transition to the more chaotic regime (i.e., to turbulent motion). Direct deposition with no flow (0 L min^{-1}) in the open chamber has also been done as a preliminary test.

The airflow directly affects the deposition rate and soot formation. The inception of soot layer formation on the substrate was perturbed by airflow rate. The mechanisms of soot formation from hydrocarbons have been discussed in several reports (Frenklach and Wang, 1991; Smooke *et al.*, 2005; Wang, 2011; Bescond *et al.*, 2016). The D1/G ratio is inversely proportional to the level of the disorder
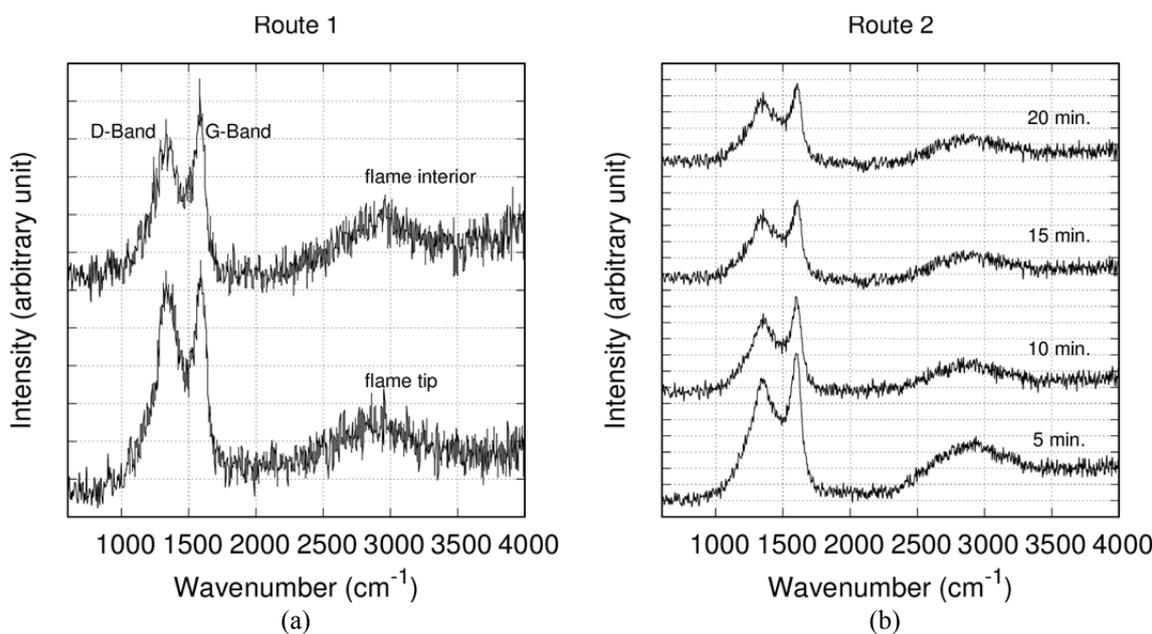

Fig. 4. Raman spectra of particle layers (a) Route 1 and (b) Route-2 originally from particles collected in the flame interior.

Table 2. Decomposition result of Raman spectrum from particle layer prepared by open chamber (0 L min^{-1}). FWHM: full width at half maximum.

Band	Peak Type	FWHM	Intensity	Center	Area (%)	Di/G
D4	Lorentz	168.8	14.3	1153.9	5.2	0.11
D1	Lorentz	217.3	131.1	1340.3	59.9	1.02
D3	Gauss	133.9	30.4	1498.2	8.8	0.23
G	Lorentz	84.9	128.4	1586.5	24.3	-
C-C*	Lorentz	110.5	7.5	1999.0	1.6	0.05
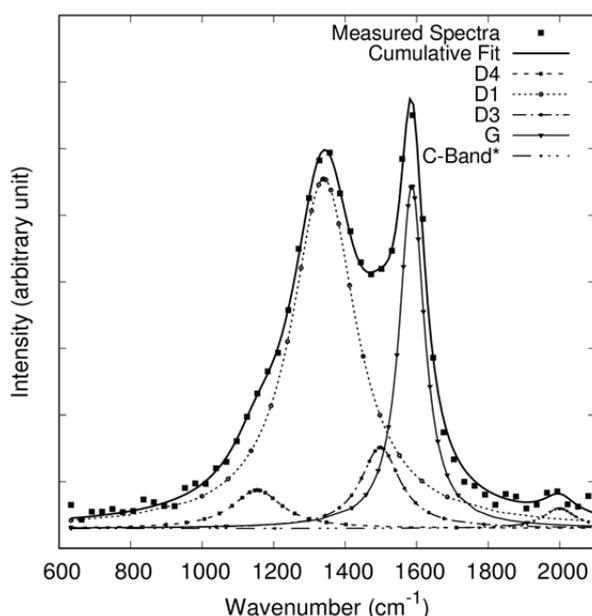
Fig. 5. Decomposition of Raman spectrum into several bands, in the case of collections, using an open-chamber flame.
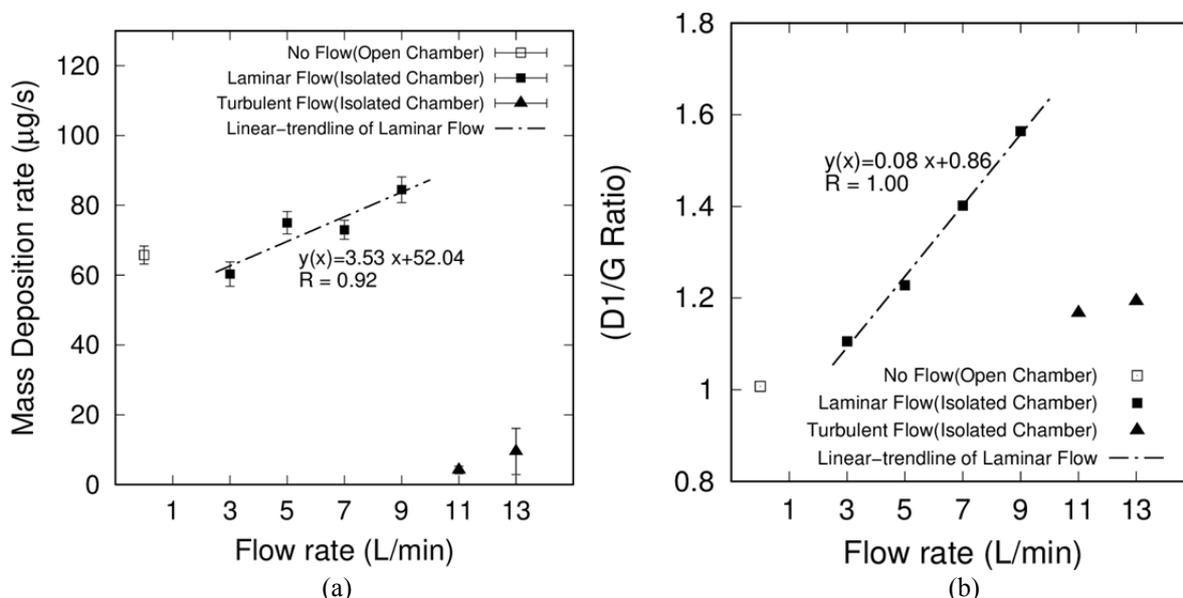
Fig. 6. (a) Mass deposition rate of soot collection vs. flow rate of air. (b) D1/G ratio of decomposed Raman spectrum vs. flow rate of air.

on graphitic phase (Ferrari and Robertson, 2000; Cançado *et al.*, 2006). From the above results, some linked relation can be identified. In steady diffusion at increasing flow-

rate of air feed from the bottom position of the candle, the deposition rate of soot particles in the collecting substrate positioned above the wick (where the inception of soot

particles happened) was increasing. This contributes linearly to the disordered degree of crystalline contained in soot particle. In a more chaotic regime (flickering flame), this statement also seems to hold.

Size Distribution of Soot Particles in Suspension

The dynamic light scattering (DLS) technique has been performed to measure particle-size distribution of the soot suspension. For the preparation of suspension, the soot particles deposited from the flame interior were used. The size distributions were measured for the soot particles suspended in ethanol and water, at different particle concentrations. It responds more strongly in the distribution width (i.e., dispersion degree of particle size).

Based on the result presented in Figs. 7(a) and 7(b) size distributions of particles from the flame interior suspended in water have narrower distribution compared to the same suspension concentration (0.044 wt %) in ethanol. It is also can be distinguished clearly from the cumulative distribution, where the point approaches 100%. The results in Figs. 7(a) and 7(b) also cover the effect of medium (water or ethanol) on the size distribution and aggregation state of particles in the suspension. At the concentration of 0.044 wt %, the micrometer-size aggregates appeared at the distribution. In lower concentration, the range of particle-size distribution also has a tendency to become narrow (Figs. 7(c) and 7(d)). Although the particle layers prepared from the interior flame are superhydrophobic in the contact angle measurement, these particles disperse well in water after ultrasonic homogenization. Considering this phenomenon, the superhydrophobicity of the particle layers may only caused by the organic content (Sahoo and Kandasubramanian, 2014)
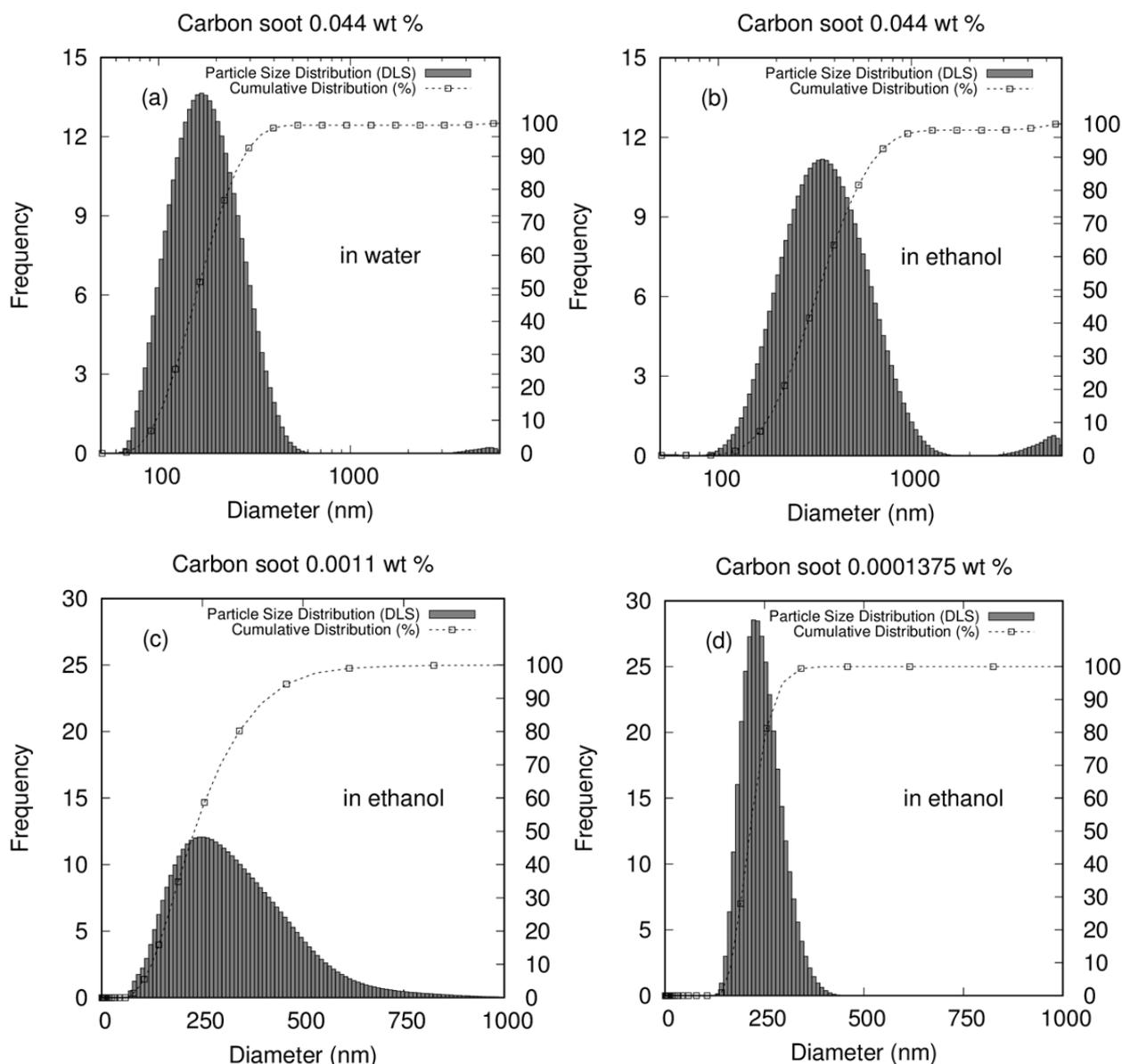
Fig. 7. Particle size distribution of 0.044 wt % (flame interior) suspension in (a) water (logarithmic × scale), (b) ethanol (logarithmic × scale). Diluted to (c) 0.0011 wt % and (d) 1.3×10^{-4} wt % in ethanol (linear × scale).

and are also contributed to by the morphological structure of the soot layer (Fig. 3, interior Route-1, and Route-2) which may not be preserved in suspension form due to ultrasonication.

Optical Properties

The optical characteristic of particle layers are measured in several conditions: after collection, in suspension, and after electrospray deposition. We measured the absorbance of the samples in the near-UV region (300–700 nm), visible (VIS), and near-infrared (NIR) wavelengths. The characteristic of the spectrum mainly differ in their steepness. The spectrum of deposited soot particle has a steep curve gradient, especially in VIS and NIR regions (Fig. 8(a)). Both spectra (flame interior and flame tip) show steep gradient directed to NIR region with different peaks.

The peak in the UV region resulting from bonding to antibonding transition (Bescond *et al.*, 2016) is observed clearly in the samples collected from the flame tip (Fig. 8(a), dashed curve). In the samples collected from the interior flame, a broader peak was observed overlapping to VIS region. The peak is extended to the VIS region in the spectrum appears to be due to electronic transition (Bescond *et al.*, 2016), and it makes the general peak shape wider in the VIS region (Fig. 8(a), solid line curve).

The same phenomena cannot be observed in the suspension state (Fig. 8(b)). The effect of solvent is too strong in the UV region. Increasing soot particle concentration only makes the intensity of absorption increase (Fig. 8(b), dashed and fine-dashed curves). We verified reappearance of the phenomena in the dry particles derived from suspension. For a comparison, we put one drop of suspension in quartz glass plate and left it dry at room temperature. The resulting spectrum is similar to originally deposited particles but with

more flat steepness toward VIS and NIR regions (Fig. 8(b), solid line curve). The reason for the steepness change is not yet understood in terms of whether it comes from dried nonvolatile matter in the solvent or change in functional group contained in the surface of the (primary) soot particles. A discussion of the interaction of ethanol with graphite surface (at low temperature) and the physisorbed of ethanol in basal plane of graphite was discussed in detail by Herwig and Trouw (1992).

The peaks at near-UV are showed a fairly sharp shape for the soot particle obtained from the flame tip. The steep condition was also found in a previous study on carbon black particle prepared by resistive heating of graphite condensed in noble gases (Jäger *et al.*, 1999). As another possibility, the responsible factor to the UV-VIS-NIR spectra is the morphological structure of the particles. As presented in Fig. 3, the degree of necking and overlapping between primary particles is increased. The contribution of overlapped and necked structure increases the absorption cross-section, which is directly proportional to the measured absorbance in the spectrum (Skorupski and Mroczka, 2014; Yon *et al.*, 2015).

CONCLUSIONS

Soot particles from the candle flame are deposited by direct exposure of the collecting glass substrate into the interior of the flame. Hydrophobic properties of freshly formed soot particle layer show a super-hydrophobic feature compared to those of the flame tip. Raman analysis indicates different intensity ratios of raw spectrum in G- and D-bands. This condition may contribute to the hydrophobic properties of the layer. The change of flow during candle burning supported by decomposition of Raman spectra
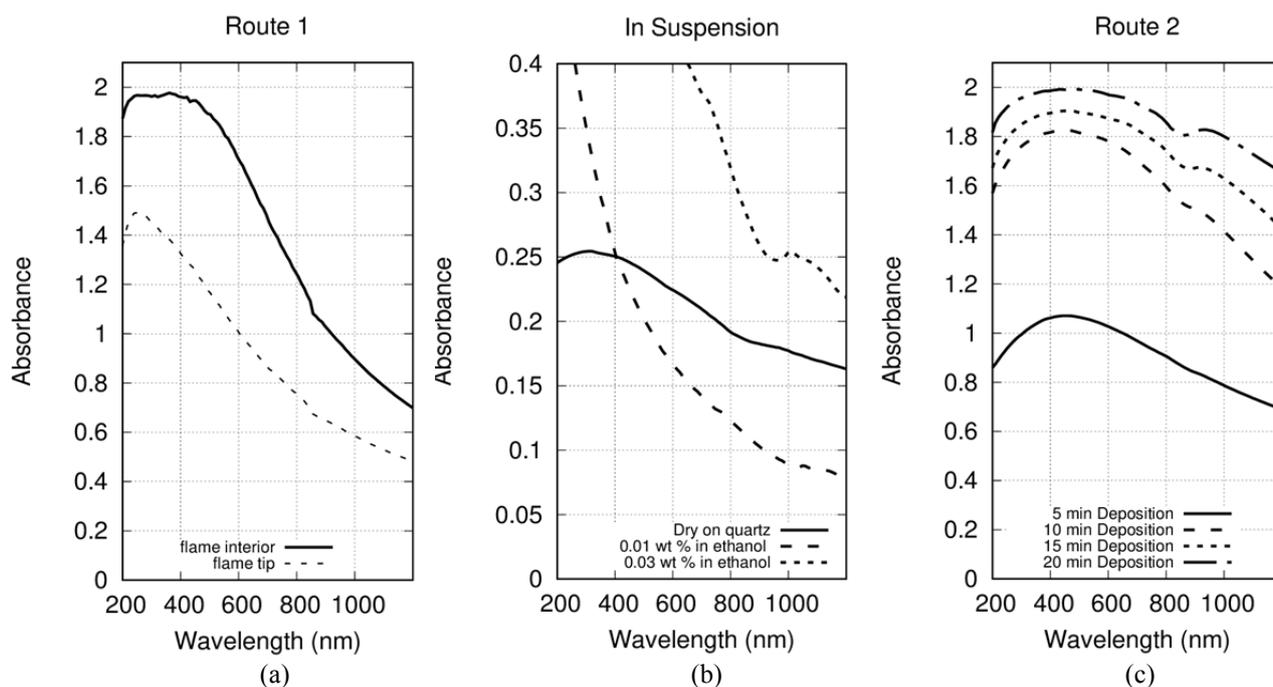
Fig. 8. Absorbance of particles (from the flame interior) in Route 1 (a), suspension in ethanol (b) and in Route 2 (c).

reveals an increasing peak (D1/G) ratio size under a steady diffusion regime. The Raman spectra between directly exposed substrate collection (Route-1) and electrospray deposition (Route-2) show no significant change in the structure of soot particles, as indicated by preservation of ratio of two main peaks (G and D). This means that charged aerosolization of electrospraying is invariant to the bond structure of soot particles suspended in the aerosol droplet. The optical characteristic shows peaks in the UV region with a steep absorbance curve spanning from UV to NIR regions, which differs based on the experimental treatment. Comparing to Route-1, deposition by electrospray (Route-2) can obtain more controllable soot particle layers.

ACKNOWLEDGMENTS

DISCLAIMER

Reference to any companies or specific commercial products does not constitute any conflict of interest.

REFERENCES

Bescond, A., Yon, J., Ouf, F.X., Rozé, C., Coppalle, A., Parent, P., Ferry, D. and Laffon, C. (2016). Soot optical properties determined by analyzing extinction spectra in the visible near-UV: Toward an optical speciation according to constituents and structure. *J. Aerosol Sci.* 101: 118–132.

Cançado, L.G., Takai, K., Enoki, T., Endo, M., Kim, Y.A., Mizusaki, H., Jorio, A., Coelho, L.N., Magalhães-Paniago, R. and Pimenta, M.A. (2006). General equation for the determination of the crystallite size la of nanographite by Raman spectroscopy. *Appl. Phys. Lett.* 88: 1–4.

Casari, C.S., Li Bassi, A., Baserga, A., Ravagnan, L., Piseri, P., Lenardi, C., Tommasini, M., Milani, A., Fazzi, D., Bottani, C.E. and Milani, P. (2008). Low-frequency modes in the Raman spectrum of sp-sp2 nanostructured carbon. *Phys. Rev. B* 77: 195444.

Chang, W.Y., Huang, W., Kim, J., Li, S. and Jiang, X. (2015). Candle soot nanoparticles-polydimethylsiloxane composites for laser ultrasound transducers. *Appl. Phys. Lett.* 107: 161903.

Commodo, M., De Falco, G., Larciprete, R., D'Anna, A. and Minutolo, P. (2016). On the hydrophilic/hydrophobic character of carbonaceous nanoparticles formed in laminar premixed flames. *Exp. Therm. Fluid Sci.* 73: 53–63.

Falcao, E.H. and Wudl, F. (2007). Carbon allotropes: Beyond graphite and diamond. *J. Chem. Technol. Biotechnol.* 82: 524–531.

Fan, M., Chen, L., Li, S., Zou, M., Su, L. and Tao, J.

(2016). The effects of morphology and water coating on the optical properties of soot aggregates. *Aerosol Air Qual. Res.* 16: 1315–1326.

Fenn, J.B., Mann, M., Meng, C.K., Wong, S.F. and Whitehouse, C.M. (1989). Electrospray ionization for mass spectrometry of large biomolecules. *Science* 246: 64–71.

Ferrari, A.C and Robertson, J. (2000). Interpretation of Raman spectra of disordered and amorphous carbon. *Phys. Rev. B* 61: 14095–14107.

Fine, P.M., Cass, G.R. and Simoneit, B.R.T. (1999). Characterization of fine particle emissions from burning church candles. *Environ. Sci. Technol.* 33: 2352–2362.

Frenklach, M. and Wang, H. (1991). Detailed modeling of soot particle nucleation and growth. *Symp. (Int.) Combust.* 23: 1559–1566.

Haynes, B.S. and Wagner, H.G. (1981). Soot formation. *Prog. Energy Combust. Sci.* 7: 229–273.

Jäger, C., Henning, T., Schlögl, R. and Spillecke, O. (1999). Spectral properties of carbon black. *J. Non-Cryst. Solids* 258: 161–179.

Kakunuri, M. and Sharma, C.S. (2015). Candle soot derived fractal-like carbon nanoparticles network as high-rate lithium ion battery anode material. *Electrochim. Acta* 180: 353–359.

Lenggoro, I.W., Xia, B., Okuyama, K. and De la Mora, J.F. (2002). Sizing of colloidal nanoparticles by electrospray and differential mobility analyzer methods. *Langmuir* 18: 4584–4591.

Liang, C.J., Liao, J.D., Li, A.J., Chen, C., Lin, H.Y., Wang, X.J. and Xu, Y.H. (2014). Relationship between wettabilities and chemical compositions of candle soots. *Fuel* 128: 422–427.

Long, C.M., Nascarella, M.A. and Valberg, P.A. (2013). Carbon black vs. black carbon and other airborne materials containing elemental carbon: Physical and chemical distinctions. *Environ. Pollut.* 181: 271–286.

Nithyanandan, K., Lin, Y., Donahue, R., Meng, X., Zhang, J. and Lee, C.F. (2016). Characterization of soot from diesel-CNG dual-fuel combustion in a {CI} engine. *Fuel* 184: 145–152.

Oh, K.C. and Shin, H.D. (2006). The effect of oxygen and carbon dioxide concentration on soot formation in non-premixed flames. *Fuel* 85: 615–624.

Osswald, S., Yushin, G., Mochalin, V., Kucheyev, S.O. and Gogotsi, Y. (2006). Control of sp2/sp3 carbon ratio and surface chemistry of nanodiamond powders by selective oxidation in air. *J. Am. Chem. Soc.* 128: 11635–11642.

Pagels, J., Wierzbicka, A., Nilsson, E., Isaxon, C., Dahl, A., Gudmundsson, A., Swietlicki, E. and Bohgard, M. (2009). Chemical composition and mass emission factors of candle smoke particles. *J. Aerosol Sci.* 40: 193–208.

Popovicheva, O.B., Kireeva, E.D., Steiner, S., Rothen-Rutishauser, B., Persiantseva, N.M., Timofeev, M.A., Shonija, N.K., Comte, P. and Czerwinski, J. (2014). Microstructure and chemical composition of diesel and biodiesel particle exhaust. *Aerosol Air Qual. Res.* 14: 1392–1401.

Ramsteiner, M., Wild, C. and Wagner, J. (1989). Interference effects in the Raman scattering intensity from thin films. *Appl. Opt.* 28: 4017.

Russo, C., Stanzione, F., Ciajolo, A. and Tregrossi, A. (2013). Study on the contribution of different molecular weight species to the absorption UV-Visible spectra of flame-formed carbon species. *Proc. Combust. Inst.* 34: 3661–3668.

Saallah, S., Naim, N.N., Mokhtar, M.N., Abu Bakar, N.F., Gen, M. and Lenggoro, W.W. (2014). Transformation of cyclodextrin glucanotransferase (CGTase) from aqueous suspension to fine solid particles via electrospraying. *Enzyme Microb. Technol.* 64–65: 52–59.

Sadezky, A., Muckenhuber, H., Grothe, H., Niessner, R. and Pöschl, U. (2005). Raman microspectroscopy of soot and related carbonaceous materials: Spectral analysis and structural information. *Carbon* 43: 1731–1742.

Sahoo, B.N. and Kandasubramanian, B. (2014). An experimental design for the investigation of water repellent property of candle soot particles. *Mater. Chem. Phys.* 148: 134–142.

Skorupski, K. and Mroczka, J. (2014). Effect of the necking phenomenon on the optical properties of soot particles. *J. Quant. Spectrosc. Radiat. Transfer* 141: 40–48.

Smooke, M.D., Long, M.B., Connelly, B.C., Colket, M.B. and Hall, R.J. (2005). Soot formation in laminar diffusion flames. *Combust. Flame* 143: 613–628.

Sovány, T., Nikowitz, K., Regdon, G., Kása, P. and Pintye-Hódi, K. (2009). Raman spectroscopic investigation of film thickness. *Polym. Test.* 28: 770–772.

Wang, H. (2011). Formation of nascent soot and other condensed-phase materials in flames. *Proc. Combust. Inst.* 33: 41–67.

Weingartner, E., Burtscher, H. and Baltensperger, U. (1997). Hygroscopic properties of carbon and diesel soot particles. *Atmos. Environ.* 31: 2311–2327.

Wu, J., Chen, L., Zhou, J., Wu, X., Gao, X., Gréhan, G. and Cen, K. (2017). Particle size distribution of soot from a laminar/diffusion flame. *Aerosol Air Qual. Res.* 17: 2095–2109.

Yang, D.S. and Zewail, A.H. (2009). Ordered water structure at hydrophobic graphite interfaces observed by 4D, ultrafast electron crystallography. *Proc. Natl. Acad. Sci. U.S.A.* 106: 4122–4126.

Yon, J., Bescond, A. and Liu, F. (2015). On the radiative properties of soot aggregates Part 1: Necking and overlapping. *J. Quant. Spectrosc. Radiat. Transfer* 162: 197–206.